Discovery of new boron-rich chalcogenides: orthorhombic B6X (X=S, Se)

Kirill Cherednichenko, Vladimir Mukhanov, Zhenhai Wang, Artem R Oganov, Aleksandr Kalinko, Iurii Dovgaliuk, Vladimir Solozhenko

Discovery of new boron-rich chalcogenides: orthorhombic B_6X (X = S, Se)

Kirill A. Cherednichenko[1], Vladimir A. Mukhanov[1], Zhenhai Wang[2,3], Artem R. Oganov[2,4,5], Aleksandr Kalinko[6,7], Iurii Dovgaliuk[8], and Vladimir L. Solozhenko[1,*]

[1] LSPM–CNRS, Université Paris Nord, Villetaneuse, 93430, France.

[2] Skolkovo Institute of Science and Technology, Skolkovo Moscow Region, 143026, Russia.

[3] Nanjing University of Posts and Telecommunications, Nanjing, Jiangsu 210003, China.

[4] Moscow Institute of Physics and Technology, Dolgoprudny City, Moscow Region 141700, Russia.

[5] School of Materials Science, Northwestern Polytechnical University, Xi'an 710072, China.

[6] Institute of Solid State Physics, University of Latvia, Riga, LV-1063, Latvia.

[7] Universität Paderborn, Naturwissenschaftliche Fakultät, Paderborn, 33098, Germany.

[8] European Synchrotron Radiation Facility, Grenoble, 38043, France.

*vladimir.solozhenko@univ-paris13.fr

ABSTRACT

New boron-rich sulfide B_6S and selenide B_6Se have been discovered from high pressure – high temperature synthesis combined with *ab initio* evolutionary crystal structure prediction, and studied by synchrotron X-ray diffraction and Raman spectroscopy at ambient condition. As it follows from Rietveld refinement of powder X-ray diffraction data, both chalcogenides have orthorhombic symmetry and belongs to *Pmna* space group. All experimentally observed Raman bands have been attributed to the theoretically calculated phonon modes, and the mode assignment has been performed. Prediction of mechanical properties (hardness and elastic moduli) of new boron-rich chalcogenides have been made using ab initio routines, and both compounds were found to be members of a family of hard phases.

Introduction

Development of modern industry requires more new materials with exceptional physical and chemical properties. Searching for such materials becomes a central challenge of modern materials science. The discoveries of fullerene, carbon nanotubes and graphene unveiled that unusual crystal structures open access to the unique properties.

Boron-rich compounds are the materials possessing such unusual structures. The B_{12} *closo*-clusters are the common feature of these compounds. Almost all boron-rich solids may be considered as a combination of 'electron deficient' B_{12}-icosahedral units (36 valence electrons over 48 bonding orbitals) and various interstitial atoms (from nonmetals to metals) as electron donors[1,2]. The polycentric metal-like bonding system within the B_{12} icosahedra and strong covalent bonds between

B_{12} *closo*-clusters and interstitial atoms makes boron-rich compounds extremely stable, which hereby leads to high melting temperatures, chemical inertness and outstanding mechanical properties[1-4]. A change of the interstitial atoms makes possible to considerably vary the properties (e.g. bulk moduli variation of α-rhombohedral boron (α-B_{12}) and isostructural boron-rich compounds: B_4C, $B_{12}O_2$, $B_{13}N_2$, $B_{12}P_2$[5,6]). Thus, a detailed study of already existing materials and exploration of new boron-rich compounds are of great importance and draw considerable attention in experiment and theory.

In the present work two new boron-rich chalcogenides were synthesized under extreme pressure–temperature conditions. Their crystal structures were found by *ab initio* crystal structure prediction, which allowed us to perform Rietveld refinement of the experimental X-ray diffraction (XRD) patterns. The Raman spectra of both boron-rich chalcogenides were acquired at ambient conditions, and the observed Raman bands were assigned to the corresponding phonon modes.

Results and Discussion

According to the energy-dispersive X-ray spectroscopy data, the elemental composition of synthesized chalcogenides is 86.1(7) at% B and 13.9(7) at% S for boron sulfide, and 86(1) at% B and 14(1) at% Se for boron selenide, so the stoichiometry of both compounds is B_6X (X = S, Se).

Crystal structure of new boron-rich sulfide and selenide. The crystal structures of new phases were predicted using the USPEX algorithm. We found that at 20 GPa the following boron-rich chalcogenides are thermodynamically stable (see thermodynamic convex hulls in Fig. 1a and Fig. 1b): B_6S, BS, B_2S_3 for boron sulfides, and B_6Se and BSe for boron selenides. The computed enthalpies of the lowest-enthalpy structures as a function of pressure are shown in Fig. 1c and Fig. 1d: B_6S with *Pmna* space group is stable in 0-20 GPa pressure range, whereas the structure of B_6Se with *Pmna* space group is stable in 4-20 GPa range.

Theoretically predicted crystal structures of boron-rich chalcogenides were further used as starting models for Rietveld refinement of the powder X-ray diffraction patterns taken at ambient conditions (Fig. 2). The backgrounds of both diffraction patterns were approximated by a 5-order polynomial. The final reliability factors R_{wp} converged to 5.0 (see Fig. 2a) and 5.8 (see Fig. 2b) indicate the excellent refinement level and, thus, confirming the correctness of the structures found with USPEX algorithm. The refined lattice parameters of boron-rich sulfide and selenide are also presented in Table 1.

The unit cell of both boron-rich chalcogenides contains 24 boron atoms in four independent (*4h* and *8i*) Wyckoff positions and 4 sulfur/selenium atoms placed in one independent (*4h*) Wyckoff position. Since all boron atoms constitute B_{12} clusters their total atom site occupancies were fixed to 1.0 by default. The total S1 and Se1 sites occupancies were found to be 0.925 and 0.952, respectively. The details of atomic structure of both compounds are presented in Table S1. Considering the occupancies of S1 and Se1 sites are close to 1, the stoichiometry of new orthorhombic boron-rich sulfide and selenide may be presented as "B_6X", where X is S or Se. It

should be underlined that the attempt to replace S and Se atoms by B atoms resulted in a large mismatching and high R_{wp} values. For convenience and in order to avoid any further confusion with previously reported hexagonal boron-rich chalcogenides (e.g. $B_{12}S_{2-x}$[7,8] and $B_{12}Se_{(2-x)}B_x$[9]) further we will call the new boron-rich sulfide and selenide as "*o*-B_6S" and "*o*-B_6Se" (where "*o*" indicates the orthorhombic symmetry). The unit cell of *o*-B_6X (where X = S, Se) is presented in Fig. 3. The X-ray densities of *o*-B_6S and *o*-B_6Se were found to be 2.54 g/cm^3 and 3.58 g/cm^3, respectively which is in good agreement with values predicted *ab initio* using USPEX (2.53 g/cm^3 and 3.55 g/cm^3) and CRYSTAL17 (2.58 g/cm^3 and 3.66 g/cm^3).

Among all experimentally obtained nonmetal boron-rich compounds only *o*-B_6S and *o*-B_6Se have the orthorhombic structure (with exception of B_6Si (*Pnnm*)[10] and B_3Si (*Imma*)[11]). The distribution/packing of the B_{12} *closo*-clusters in *o*-B_6X (X = S, Se) unit cells may be described as side-centered (Fig. 3) similar to that in B_3Si. One slightly distorted B_{12}-icosahedron in *o*-B_6S and *o*-B_6Se is linked with six others. The lengths of intra-icosahedral B–B bonds vary from 1.7294 Å to 1.8987 Å in *o*-B_6S and from 1.7077 Å to 1.9009 Å in *o*-B_6Se, whereas the inter-icosahedral bond lengths in *o*-B_6S and *o*-B_6Se are: 1.6949 Å (B1–B1), 1.7448 Å (B2–B2), and 1.7511 Å (B1–B1), 1.8004 Å (B2-B2) respectively. One sulfur/selenium atom is linked with three closest icosahedra: S1–B4 (1.8884 Å), S1–B3 (1.8586 Å), Se1–B3 (1.9623 Å) and Se1–B4 (2.0128 Å).

The predicted lattice parameters and mechanical properties, as well as atoms positions of new boron-rich chalcogenides are presented in Table 1 and Table S1. Both phases are considerably more compressible (B_0 values estimated by VASP and CRYSTAL17 are in good agreement) and less hard than γ-B_{28}[12,13], α-rhombohedral boron[14-16] and isostructural boron-rich compounds[5,6,17-21].

Raman spectra of new boron-rich sulfide and selenide. *o*-B_6S and *o*-B_6Se have 28 atoms in the unit cell, thus, 84 normal modes are expected. According to the symmetry analysis, the acoustic and optic modes of *o*-B_6X (where X = S or Se) at Γ point can be presented as follows:

$$\Gamma_{acoustic} = B_{1u} + B_{2u} + B_{3u}$$

$$\Gamma_{optic} = 12A_g + 9A_u + 9B_{1g} + 11B_{1u} + 9B_{2g} + 11B_{2u} + 12B_{3g} + 8B_{3u}$$

$11B_{1u} + 11B_{2u} + 8B_{3u}$ are IR active modes; $12A_g + 9B_{1g} + 9B_{2g} + 12B_{3g}$ are Raman active modes; others are silent modes.

Raman spectra of *o*-B_6S and *o*-B_6Se were measured in the 100-2500 cm^{-1} frequency range, however, all bands were observed in the 150-1100 cm^{-1} region (Fig. 4). The Raman spectra of *o*-B_6S and *o*-B_6Se resemble the Raman spectra of α-B_{12}[22,23] and γ-B_{28}[24] and other boron-rich compounds[25-28]. The most intense and narrow bands are situated in the low-frequency region (<500 cm^{-1} for *o*-B_6S and <400 cm^{-1} for *o*-B_6Se), whereas the less intense and broad bands and band groups are concentrated in the high-frequency region.

The CRYSTAL17 and VASP calculated Raman spectra of both compounds (at T = 0 K) are presented in Fig. 4 and Fig. S1, respectively. The theoretically predicted Raman active phonon

modes (ω_t^C and ω_t^V, for CRYSTAL17 and VASP, respectively), experimentally observed Raman bands and overlapped band groups (ω_0) of *o*-B_6S and *o*-B_6Se are listed in Table S2. The theoretical and experimental data were found to be in a good agreement. The average error on individual modes being less than 1.5% for *o*-B_6S (with a maximum error of 2.8%; mode at 780 cm^{-1}) and 1.2% for *o*-B_6S (with a maximum error of 2.7%; mode at 594 cm^{-1}). A good agreement between theory and experiment (also observed in our previous Raman studies[29,30]) gave us confidence in the predictive power of our *ab initio* calculations for the modes assignment (see Table S2).

The predicted phonon modes were confidently associated with the corresponding atomic movements in *o*-B_6S and *o*-B_6Se unit cells with help of visualization procedure built in MOLDRAW software[31]. Taking into account that normal modes of boron-rich chalcogenides with such complicated structure may incorporate various simultaneous atomic movements, we distinguished the most distinct ones only for the convenience of the further modes description. As one can see in Fig. 4, the Raman bands of both spectra were divided onto four groups (*G1 – G4*).

The "*G1*" contains the low frequency modes (280-400 cm^{-1} for *o*-B_6S and 150-280 cm^{-1} for *o*-B_6Se) referred to the symmetric and antisymmetric oscillations (e.g. rocking, twisting, wagging) of S/Se atoms and the corresponding B_{12}–icosahedral units distortions.

The Raman bands of group "*G2*" (420-520 cm^{-1} for *o*-B_6S and 330-500 cm^{-1} for *o*-B_6Se) were associated with various tilting oscillations of the whole B_{12} units around different crystallographic [100], [010] and [001] directions (rocking and wagging of the equatorial and polar boron atoms of one B_{12}-unit). Unlike Se atoms, the oscillations of S atoms were found rather significant in some "*G2*" modes. This phenomenon can be easily explained by the atomic mass difference of S and Se atoms.

The middle-frequency modes in "*G3*" (550-760 cm^{-1} for *o*-B_6S and 550-740 cm^{-1} for *o*-B_6Se) were referred, first of all, to different vibrations of the equatorial B atoms (B2 - B4) leading to stretching of the intra-icosahedral B–B bonds, rotations of the B1–B1 and B2–B2 inter-icosahedral bonds and rotations, twisting and "parasol" oscillations of the S–$(B)_3$ structural elements (three B atoms belong to three different B_{12}-units).

The "*G4*" group contains the high-frequency modes (760-1100 cm^{-1} for *o*-B_6S and 740-1050 cm^{-1} for *o*-B_6Se) described by oscillations of the equatorial and polar born atoms of B_{12} units leading to stretching of the inter-icosahedral bonds (B–Se, B2–B2, B1–B1). For instance, in both spectra the two phonon modes with the highest frequencies correspond to the oscillations of the polar B1 atoms and, thus, to the stretching of the B1–B1 inter-icosahedral bonds.

Such a division of *o*-B_6S and *o*-B_6Se normal modes is consistent with previously reported classification of vibrational modes of α-B_{12} and isostructural boron-rich compounds[22,23,26,27]: the modes involving the whole icosahedron rotations lay in the 100-200 cm^{-1} range, intra-icosahedral modes lay between 550-950 cm^{-1}, and inter-icosahedral modes with wave numbers above 1000 cm^{-1}.

The detailed explanation of the bands widths over ~600 cm^{-1} requires additional XRD and Raman studies of *o*-B_6S and *o*-B_6Se single crystals (perhaps coupled with low-temperature and high-pressure measurements). Nonetheless, it might be assumed, that some random distortions of B_{12}-icosahedral units (not detectable by powder XRD) and, thus, corresponding distortion of the intra- and inter-icosahedral bonds as well as partial occupation of *4h* sites by S/Se atoms might be the most probable reasons of the observed Raman bands broadening. Earlier, the isotopic $^{11}B/^{10}B$ disorder in α-boron was also proposed as a possible reason of the Raman bands broadening[23].

To conclude, in the present work new boron-rich sulfide *o*-B_6S and selenide *o*-B_6Se were synthesized under extreme *p-T* conditions and studied by powder X-ray diffraction and Raman spectroscopy at ambient pressure. With help of *ab initio* evolutionary crystal structure predictions combined with Rietveld refinement of synchrotron X-ray diffraction data, the crystal structures of the boron-rich chalcogenides were refined. Both phases have orthorhombic symmetry and belong to the same space group *Pmna* (53). The observed Raman bands were assigned to the phonon modes and associated with atomic movements. Elastic properties of new boron-rich chalcogenides were theoretically predicted using various *ab initio* routines.

Methods

Experimental. Formation of new boron-rich chalcogenides was first observed in our *in situ* high pressure – high temperature studies of the B–S and B–Se binary systems at BL04B1 beamline, SPring-8 (Japan) and PSICHE beamline, SOLEIL (France). Chemical interaction of elemental boron with sulfur and selenium melts were studied by energy-dispersive X-ray diffraction at pressures up to 11 GPa and temperatures up to 2500 K using SPEED-1500 multianvil press (BL04B1) and Paris-Edinburgh press (PSICHE) using white beam (20-150 keV, bending magnet @ BL04B1; 25-80 keV, wiggler source @ PSICHE).

Based on the information about the most appropriate synthesis conditions and optimal stoichiometries of B:S(Se) reaction mixtures extracted from our synchrotron studies, the new boron-rich chalcogenides have been synthesized at 6.1 GPa and 2700 K in a toroid-type high-pressure apparatus. A design of the high-temperature assembly used in recovery experiments is described elsewhere[32]. The powders of amorphous boron (Grade I ABCR), and sulfur and selenium (both Alfa Aesar, 99.5%) were used as starting materials. Boron nitride capsules (COMPRES) were used to isolate the reaction mixture (B:X molar ratio 5:1) from the graphite heater. The recovered samples were grinded in mortar and treated with 3N nitric acid (ACS, Alfa Aesar) for 20 min at 370 K in order to remove unreacted boron, washed with deionized water and dried at 400 K. The chemical composition of synthesized compounds was studied by energy-dispersive X-ray spectroscopy using scanning electron microscope FEI Quanta 200F at 10 kV accelerating voltage (see. Fig. S2).

X-ray diffraction study of boron-rich chalcogenides was performed at Swiss-Norwegian Beamline BM01, ESRF[33]. The wavelength of monochromatic beam from a bending magnet was set to 0.6866 Å. X-ray diffraction patterns were collected during 20 s in Debye-Scherrer geometry with

rotating quartz-glass capillary using PILATUS 2M detector. The crystal structure refinement was performed using Maud software[34]; high purity LaB_6 was used as a standard.

Raman spectra of powder polycrystalline samples were measured in different spatial points at ambient conditions in the 100-2000 cm^{-1} range using Horiba Jobin Yvon HR800 Raman spectrometer; the spectrometer was calibrated using single-crystal cubic Si at room temperature. Unpolarized light from 633-nm line of He-Ne laser (10 μm beam spot) was used for excitation. The measurements were also performed at 473-nm excitation wavelength; no resonant effects and/or significant photoluminescence were observed (Fig. S1).

Computational Details. X-ray diffraction patterns of the newly synthesized phases clearly did not match any previously known phases. Neither their structures, nor the exact chemical compositions were known. Taking into account the starting B:S/Se molar ratios we assumed the probable composition as: B_xS and B_xSe with $5 \le x \le 7$. This information was insufficient for the determination of the crystal structures solely from experiment.

We performed variable-composition searches for all stable compounds in the B-S and B-Se systems using the USPEX code[35-37], which has already demonstrated exceptional predictive power, reliability and efficiency for discovering novel compounds and their crystal structures (e.g. [38-41]). Searches were performed at the pressure of 20 GPa, the initial population was made of structures containing up to 30 atoms in the primitive unit cell. In each generation there were 60 structures, and calculations were run for 60 generations. All produced structures were carefully relaxed and their enthalpies were computed using the Vienna *ab initio* Simulation Package (VASP)[42] within the generalized gradient approximation (GGA) of Perdew-Burke-Ernzerhof (PBE)[43]. Total energy was calculated within the framework of projector augmented wave (PAW) method[44]. We used plane wave energy cutoff of 550 eV and Gamma-centered *K*-point mesh with the resolution of $2\pi \cdot 0.06 Å^{-1}$ for final structural relaxations in USPEX. For mechanical and electronic property calculations, we improved the *K*-point mesh to the resolution of $2\pi \cdot 0.04 Å^{-1}$. Vickers hardness was estimated using Chen[45] and Mazhnik-Oganov[46] models, while the fracture toughness was calculated by Niu-Oganov[47] and Mazhnik-Oganov[46] models. The most reliable results should be expected from Mazhnik-Oganov models, and the discrepancy between the used models gives an idea of the results uncertainty.

The Raman spectra of both boron-rich chalcogenides were computed using VASP code with the fully relaxed structure. Firstly, we performed phonon calculation to determine phonon frequencies and normal modes at the Γ-point based on density functional perturbation theory (DFPT) as implemented in the PHONOPY code. Further DFPT method was used to compute out macroscopic dielectric tensor. And lastly, Raman intensity for each normal mode was obtained by calculating the derivative of the calculated macroscopic dielectric tensor (or polarizability) with respect to the corresponding normal mode coordinate.

At the same time, structural and phonon properties of both boron-rich chalcogenides were also studied using linear combination of atomic orbital (LCAO) calculations based on the hybrid

exchange-correlation density functional (DFT)/Hartree-Fock (HF) scheme, which is implemented in CRYSTAL17 code[48]. For boron and sulfur atoms we used all electron basis sets which were optimized in earlier calculations[49,50]48. The core electrons of the selenium atoms were excluded from consideration using the effective core pseudopotential (ECP) with corresponding atomic basis set[50]. The accuracy of the calculation of the bielectronic Coulomb and exchange series is controlled by the set of tolerances, which were taken to be 10^{-7}, 10^{-7}, 10^{-7}, 10^{-9}, and 10^{-30}, according to the recommendation for hybrid functionals[50]. The Monkhorst-Pack scheme[51] for an 8×8×8 k-point mesh in the Brillouin zone was applied. Self-consistent field calculations were performed for hybrid DFT/HF WCGGA-PBE-16% functional[52]. The percentage 16% defines the Hartree-Fock admixture in the exchange part of DFT functional.

The full structure optimization procedure according to the energy minima criterion was performed for both boron-rich chalcogenides. The bulk moduli of both compounds were estimated using routine implemented in CRYSTAL17 code[53]. The unit cell volumes were varied from 95% to 105% of the volume (V_0) corresponding to the energy minimum (E_0). The structure optimization was performed at each volume value. The obtained E(V) dependences were fitted to the Birch-Murnaghan equation of state.

The phonon frequencies for both compounds were calculated using the direct (frozen-phonon) method implemented in CRYSTAL17 code[54,55]. Calculation of Raman intensities was performed by using a coupled-perturbed Hartree–Fock/Kohn–Sham approach[55,56]. Raman spectra were constructed by using the transverse optical (TO) modes and by adopting a pseudo-Voigt functional form[54] with a full width half maximum parameter set to 1. The choice of the broadening was determined according to the criteria to keep maximal possible small intensity bands in theoretical spectrum, which are smeared out while applying higher broadening parameters.

References

1. Emin, D. Icosahedral boron-rich solids. *Phys. Today* **40**, 55-62 (1987).
2. Albert, B., Hillebrecht, H. Boron: Elementary challenge for experimenters and theoreticians. *Angew. Chem. Int. Ed.* **48**, 8640-8668 (2009).
3. Emin, D. Unusual properties of icosahedral boron-rich solids. *J Solid State Chem.* **179**, 2791-2798 (2006).
4. Carrard, M., Emin, D., Zuppiroli, L. Defect clustering and self-healing of electron-irradiated boronrich solids." *Phys Rev B* **51**, 11270 (1995).
5. Cherednichenko, K.A. & Solozhenko, V.L. Structure and equation of state of tetragonal boron subnitride $B_{50}N_2$. *J Appl. Phys.*, **122**, 155901 (2017).
6. Cherednichenko, K.A., Le Godec, Y., Solozhenko, V.L. Equation of state of boron subarsenide $B_{12}As_2$ to 47 GPa. *High Pres. Res.* **38**, 224-231 (2018).
7. Lundstrom, T. Structure and bulk modulus of high-strength boron compounds. *J. Solid State Chem.* **133**, 88-92 (1997).
8. Sologub, O., Matsushita, Y., Mori, T. An α-rhombohedral boron-related compound with sulfur: Synthesis, structure and thermoelectric properties. *Scr. Mater* **68**, 289-292 (2013).
9. Bolmgren, H. & Lundstrom, T. The crystal structure of a new boron selenide, $B_{12}S_{2-x}B_x$. *J. Alloy Compd.* **202**, 73-76 (1993).
10. Vlasse, M. The crystal structure of SiB_6. *J. Solid. State Chem.* **63**, 31-45 (1986).
11. Salvador, J.R., Bilc, D., Mahanti, S.D., Kanatzidis, M.G. Stabilization of β-SiB_3 from liquid Ga: A boron-rich binary semiconductor resistant to high-temperature air oxidation. *Angew. Chem. Int. Ed.* **42**, 1929-1932 (2003).
12. Solozhenko, V.L., Kurakevych, O.O., Oganov, A.R. On the hardness of a new boron phase, orthorhombic γ-B_{28}. *J. Superhard Mater.* **30**, 428-429 (2008).
13. Le Godec, Y., Kurakevych, O.O., Munsch, P., Garbarino, G., Solozhenko, V.L. Equation of state of orthorhombic boron, γ-B_{28}. *Solid State Comm.* **149**, 1356-1358 (2009).
14. Amberger, E. & Stumpf, W. Boron. *Gmelin Handbook of Inorganic Chemistry*, Berlin: Springer Verlag, 112-238 (1981).
15. Nelmes, R.J., Loveday, J.S., Allan, D.R., Besson, J.M., Hamel, G., Grima, P., Hull, S. Neutron- and X-ray-diffraction measurements of the bulk modulus of boron. *Phys Rev B.* **47**, 7668-7673 (1993).
16. Chuvashova, I., Bykova, E., Bykov, M., Svitlyk, V., Gasharova, B., Mathis, Y.L., Caracas, R., Dubrovinsky, L., Dubrovinskaia, N. High-pressure behavior of α-boron studied on single

crystals by X-ray diffraction, Raman and IR spectroscopy. *J. Solid State Chem.* **245**, 50-60 (2017).

17. Slak, G.A. & Morgan, K.E. Some crystallography, chemistry, physics, and thermodynamics of $B_{12}O_2$, $B_{12}P_2$, $B_{12}As_2$, and related alpha-boron type crystals. *J. Phys. Chem. Solids* **75**, 1054-1074 (2014).

18. Solozhenko, V.L. & Kurakevych, O.O. 300-K equation of state of rhombohedral boron subnitride, $B_{13}N_2$. *J. Solid State Chem.* **149**, 2169-2171 (2009).

19. Solozhenko, V.L., Cherednichenko, K.A., Kurakevych, O.O. Thermoelastic equation of state of boron subphosphide $B_{12}P_2$. *J. Superhard Mater.* **39**, 71-74 (2017).

20. Dera, P., Manghnani, M.H., Hushur, A., Hu, Y., Tkachev, S. New insights into the enigma of boron carbide inverse molecular behavior. *J. Solid State Chem.* **215**, 85-93 (2014).

21. Chuvashova, I., Bykova, E., Bykov, M., Svitlyk, V., Dubrovinsky, L., Dubrovinskaia, N. Structural stability and mechanism of compression of stoichiometric $B_{13}C_2$ up to 68GPa. *Sci. Rep*. **7**, 8969 (2017).

22. Beckel, C.H., Yousaf, M., Fuka, M.Z., Raja, S.Y.R. Lu, N. Lattice vibrations of the icosahedral solid α-boron. *Phys. Rev. B* **44**, 2535-2553 (1991).

23. Vast, N., Baroni, S., Zerah, G., Besson, J.M., Polian, A., Grimsditch, M., Chervin, J.C. Lattice dynamics of icosahedral α-boron under pressure. *Phys. Rev. Lett.* **78**, 693-696 (1997).

24. Zarechnaya, E.Yu., Dubrovinskaia, N., Dubrovinsky, L. Polarized Raman spectroscopy of high-pressure orthorhombic boron phase. *High Pres. Res.* **29**, 530-535 (2009).

25. Shelnutt, J.A., Morosin, B., Emin, D., Mullendore, A., Slack, G., Wood, C. Raman spectroscopy of boron carbides and related boron containing materials. *AIP Conf. Proc.* **140**, 312-324 (1986).

26. Tallant, D.R., Aselage, T.L., Campbell, A.N., Emin, D. Boron carbide structure by Raman spectroscopy. *Phys. Rev. B* **40**, 5649-5656 (1989).

27. Aselage, T.L., Tallant, D.R., Emin, D. Isotope dependencies of Raman spectra of $B_{12}As_2$, $B_{12}P_2$, $B_{12}O_2$, and $B_{12+x}C_{3-x}$: Bonding of intericosahedral chains. *Phys. Rev. B* **56**, 3122-3129 (1997).

28. Werheit, H., Filipov, V., Kuhlmann, U., Schwarz, U., Armbrüster, M., Leithe-Jasper, A., Tanaka, T., Higashi, I., Lundström, T., Gurin, V.N., Korsukova, M.M. Raman effect in icosahedral boron-rich solids. *Sci. Technol. Adv. Mater.* **11**, 023001 (2010).

29. Cherednichenko, K.A., Sokolov, P.S., Kalinko, A., Le Godec, Y., Polian, A., Itié, J.P., Solozhenko, V.L. Optical phonon modes in rhombohedral boron monosulfide under high pressure. *J. Appl. Phys.* **117**, 185904 (2015).

30. Cherednichenko, K.A., Le Godec, Y., Kalinko, A., Mezouar, M., Solozhenko, V.L. Orthorhombic boron oxide under pressure: In situ study by X-ray diffraction and Raman scattering. *J. Appl. Phys.* **120**, 175901 (2016).

31. Ugliengo, P., Viterbo, D., Chiari, G. MOLDRAW: Molecular Graphics on a Personal Computer. *Z. Kristallogr*. **207**, 9-23 (1993).

32. Mukhanov, V.A., Sokolov, P.S., Solozhenko, V.L. On melting of B_4C boron carbide under pressure. *J. Superhard Mater.* **34**, 211-213 (2012).

33. Dyadkin, V., Pattison, P., Dmitriev, V., Chernyshov, D. A new multipurpose diffractometer PILATUS@SNBL. *J. Synchrotron Rad.* **23**, 825-829 (2016).

34. Lutterotti, L., Bortolotti, M., Ischia, G., Lonardelli, I., Wenk, H.-R. Rietveld texture analysis from diffraction images *Z. Kristallogr. Suppl.* **26**, 125-130 (2007).

35. Oganov, A.R. & Glass, C.W. Crystal structure prediction using *ab initio* evolutionary techniques: Principles and applications. *J. Chem. Phys.* **124**, 244704 (2006).

36. Oganov, A.R., Lyakhov, A.O., Valle, M. How evolutionary crystal structure prediction works-and why. *Acc. Chem. Res.* **44**, 227-237 (2011).

37. Lyakhov, A.O., Oganov, A.R., Stokes, H., Zhu, Q. New developments in evolutionary structure prediction algorithm USPEX. *Comp. Phys. Comm.* **184**, 1172-1182 (2013).

38. Zhang, W.W., Oganov, A.R., Goncharov, A.F., Zhu, Q., Boulfelfel, S.E., Lyakhov, A.O., Stavrou, E., Somayazulu, M., Prakapenka, V.B., Konopkova, Z. Unexpected stoichiometries of stable sodium chlorides. *Science* **342**, 1502-1505 (2013).

39. Li, Y.L., Wang, S.N., Oganov, A.R., Gou, H., Smith, J.S., Strobel, T.A. Investigation of exotic stable calcium carbides using theory and experiment. *Nature Comm.* **6**, 6974 (2015).

40. Cherednichenko, K.A., Kruglov, I.A., Oganov, A.R., Le Godec, Y., Mezouar, M., Solozhenko, V.L. Boron monosulfide: equation of state and pressure-induced phase transition. *J. Appl. Phys*. **123**, 135903 (2018).

41. Kruglov, I.A., Kvashnin, A.G., Goncharov, A.F., Oganov, A.R., Lobanov, S.S., Holtgrewe, Jiang, N., Prakapenka, V.B., Greenberg, E., Yanilkin, A.V. Uranium polyhydrides at moderate pressures: Prediction, synthesis, and expected superconductivity. *Sci. Adv.* **4**, eaat9776 (2018).

42. Kresse, G. & Furthmuller, J. Efficient iterative schemes for *ab initio* total-energy calculations using a plane-wave basis set. *Phys. Rev. B* **54**, 11169-11186 (1996).

43. Perdew, J., Burke, K., Ernzerhof, M. Generalized gradient approximation made simple. *Phys. Rev. Lett.* **77**, 3865-3868 (1996).

44. Kresse, G. & Joubert, D. From ultrasoft pseudopotentials to the projector augmented-wave method. *Phys. Rev. B* **59**, 1758-1775 (1999).

45. Chen, X., Niu, H., Li, D., Li, Y. Modeling hardness of polycrystalline materials and bulk metallic glasses. *Intermetallics*, **19**, 1275-1281 (2011).

46. Mazhnik, E., Oganov, A.R. A model of hardness and fracture toughness of solids. *J. Appl. Phys.* **126**, 125109 (2019).

47. Niu, H., Niu, S., Oganov, A.R. Simple and accurate model of fracture toughness of solids. *J. Appl. Phys.* **125**, 065105 (2019).

48. Dovesi, R., Erba, A., Orlando, R., Zicovich-Wilson, C.M., Civalleri, B., Maschio, L., Rerat, M., Casassa, S., Baima, J., Salustro, S., Kirtman, B. Quantum-mechanical condensed matter simulations with CRYSTAL. *WIREs Comput Mol Sci.* **8**, e1360 (2018).

49. Orlando, R., Dovesi, R., Roetti, C. Ab initio Hartree-Fock calculations for periodic compounds: application to semiconductors. *J. Phys.: Condens. Matter* **2**, 7769-7789 (1990).

50. Heyd, J., Peralta, J.E., Scuseria, G.E., Martin, R.L. Energy band gaps and lattice parameters evaluated with the Heyd-Scuseria-Ernzerhof screened hybrid functional. *J. Chem. Phys.* **123**, 174101 (2005).

51. Monkhorst, H.J. & Pack, J.D. Special points for Brillouin-zone integrations. *Phys. Rev. B* **13**, 5188-5192 (1976).

52. Wu, Z. & Cohen, R.E. More accurate generalized gradient approximation for solids. *Phys. Rev. B* **73**, 235116 (2006).

53. Erba, A., Mahmoud, A., Belmonte, D., Dovesi, R. High pressure elastic properties of minerals from *ab initio* simulations: The case of pyrope, grossular and andradite silicate garnets. *J. Chem. Phys.* **140**, 124703 (2014).

54. Dovesi, R., Saunders, V.R., Roetti, C., Orlando, R., Zicovich-Wilson, C.M., Pascale, F., Civalleri, B., Doll, K., Harrison, N.M., Bush, I.J., D'Arco, P., Llunell, M., Causà, M., Noël, Y., Maschio, L., Erba, A., Rerat M., Casassa, S. CRYSTAL17 User's Manual (University of Torino, Torino, 2017).

55. Pascale, F., Zicovich-Wilson, C.M., Lopez, F., Civalleri, B., Orlando, R., Dovesi, R. The calculation of the vibrational frequencies of crystalline compounds and its implementation in the CRYSTAL code. *J. Comput. Chem.* **25**, 888-897 (2004).

56. Zicovich-Wilson, C.M., Pascale, F., Roetti, C., Saunders, V.R., Orlando, R., Dovesi, R. The calculation of the vibration frequencies of alpha-quartz: the effect of hamiltonian and basis set. *J. Comput. Chem.* **25**, 1873-1881 (2004).

Acknowledgements

The authors thank T. Chauveau (LSPM) for help with Rietveld analysis, A. Jamali (LRCS) for assistance with SEM measurements, and Drs. Y. Tange (SPring-8) and N. Guignot (SOLEIL) for help in synchrotron experiments that were carried out during beamtimes allocated to proposals 2017A1047 & 2018A1121 at SPring-8 and proposal 20170092 at SOLEIL. *Ab initio* calculations have been performed using Rurik and Arkuda supercomputers.

This work was financially supported by the European Union's Horizon 2020 Research and Innovation Programme under Flintstone2020 project (grant agreement No. 689279). Z.W. thanks the National Science Foundation of China (grant No. 11604159). A.R.O. thanks the Russian Science Foundation (grant 16-13-10459).

Author contributions statement

V.L.S. designed and directed the study. K.A.Ch., V.L.S. and I.D. carried out synchrotron experiments. V.A.M. and V.L.S. performed HP-HT synthesis. Z.W. and A.R.O. did crystal structure prediction and conducted VASP calculations. A.K. performed LCAO calculations. K.A.Ch. and V.L.S. analyzed the experimental data. Manuscript draft was prepared by K.A.Ch.; all authors discussed the results and contributed to writing and editing.

Competing interests

The authors have no competing interests as defined by Nature Publishing group, or other interests that might be perceived to influence the results and /or discussion reported in this paper.

Table 1. Unit cell parameters (a_0, b_0, c_0) and predicted mechanical properties of *o*-B_6X (X = S, Se): bulk modulus (B_0), shear modulus (G), Young's modulus (E), Poisson's ratio (v), Vicker's hardness (H_V) and fracture toughness (K_{Ic}).

	o-B_6S (*Pmna*)			*o*-B_6Se (*Pmna*)		
	Exp.	VASP	CRYSTAL17	Exp.	VASP	CRYSTAL17
a_0, Å	5.8170(1)	5.8307	5.8139	5.9463(1)	5.9684	5.9359
b_0, Å	5.3025(1)	5.3202	5.2918	5.3579(1)	5.3802	5.3416
c_0, Å	8.2135(1)	8.2072	8.2026	8.3824(1)	8.3809	8.3631
V_0, Å^3	253.34(1)	254.59	252.36	267.06(1)	269.12	265.17
B_0, GPa	—	146	151	—	137	144
G, GPa	—	138	—	—	135	—
E, GPa	—	315	—	—	304	—
v	—	0.14	—	—	0.13	—
H_V, GPa	—	31[a] 24[b]	—	—	32[a] 24[b]	—
K_{Ic}, MPa·m$^{1/2}$	—	2.1[c] 1.5[d]	—	—	2.0[c] 1.2[d]	—

[a] Chen model [45]

[b] Mazhnik-Oganov model [46]

[c] Niu-Oganov model [47]

[d] Mazhnik-Oganov model [46]

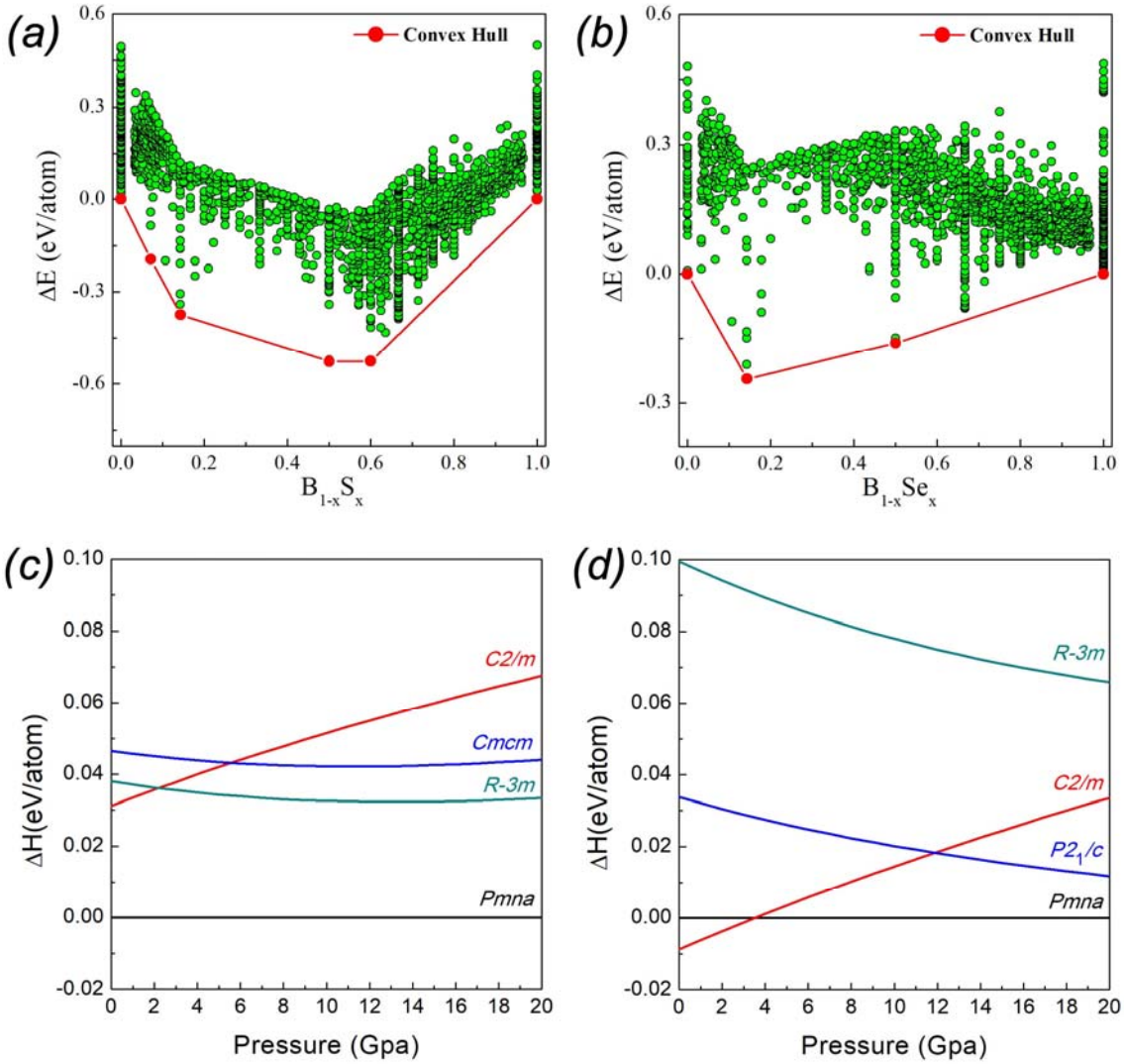

Figure 1 Convex hull of B-S (*a*) and B-Se (*b*) variable-composition USPEX calculations at 20 GPa. Enthalpy difference (ΔH) between stable/metastable B_6S (*c*) and B_6Se (*d*) structures in the 0-20 GPa pressure range.

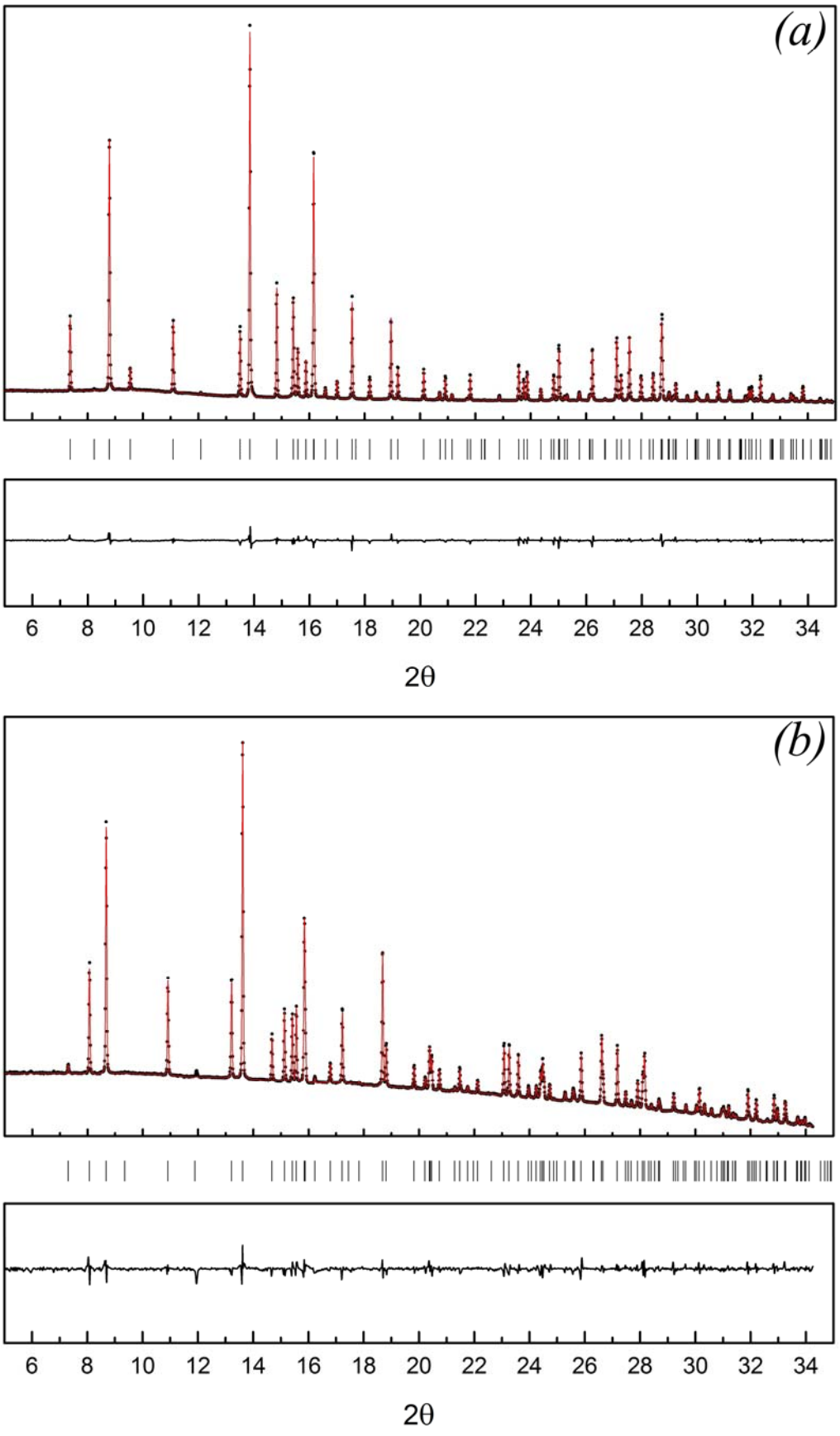

Figure 2 Rietveld full profile refinement of powder X-ray diffraction patterns of *o*-B_6S (*a*) and *o*-B_6Se (*b*).

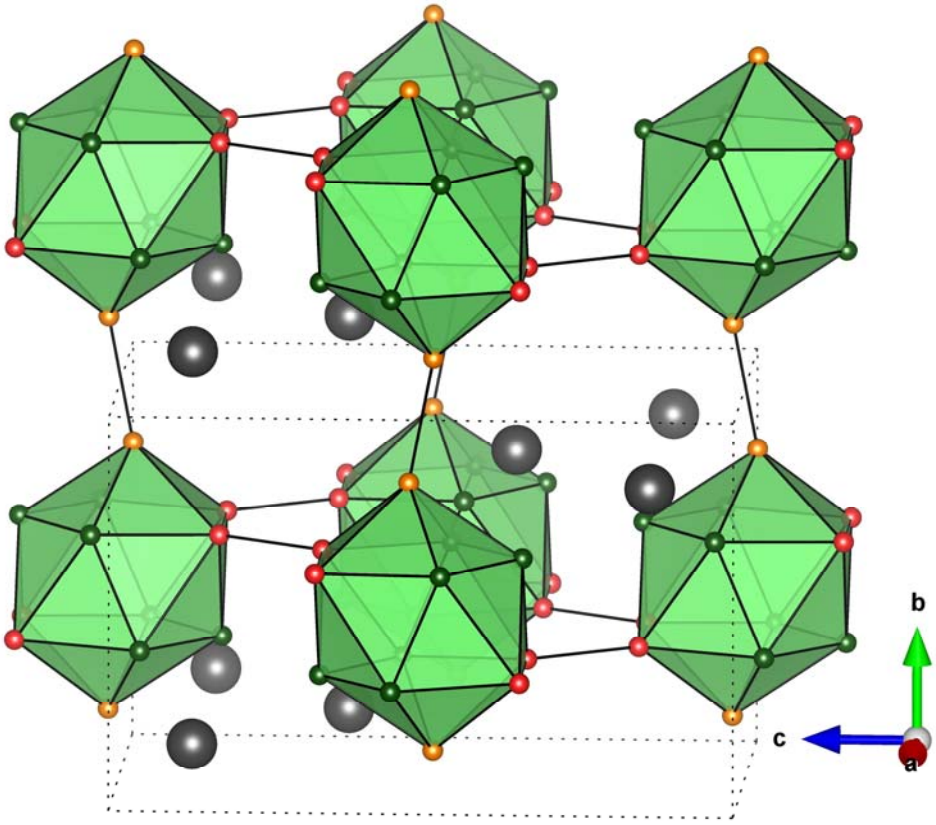

Figure 3 Crystal structure of new orthorhombic phases of boron-rich sulfide and selenide, *o*-B_6X (B_{12}-units are presented by green icosahedral polyhedral; polar B1; equatorial B2 and B3; and B4 atoms are marked by orange, red and green balls, respectively; X = S, Se atoms are shown as large grey balls).

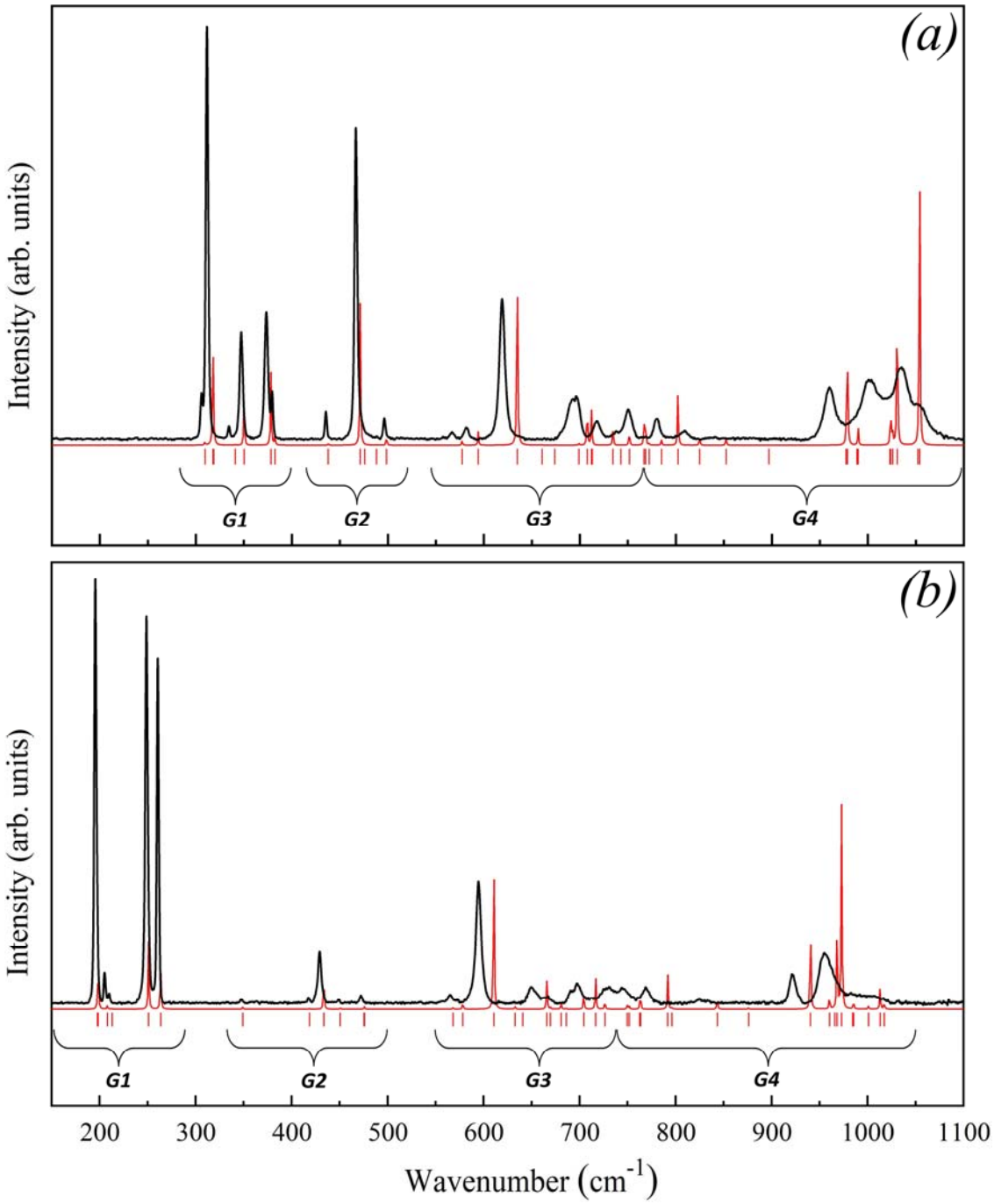

Figure 4 The experimental (black) and calculated by CRYSTAL17 (red) Raman spectra of *o*-B_6S (*a*) and *o*-B_6Se (*b*). The red dashes show all predicted Raman active phonon modes.